Doctoral Dissertation

Efficient recombinant production of mouse-derived cryptdin family peptides by a novel facilitation strategy for inclusion body formation

（新規封入体形成促進技術によるマウス由来 cryptdin ファミリーペプチドの組換え体の効率的生産）

Yuchi Song

Graduate School of Life Science, Hokkaido University

2023.3

Contents

Abstract

Antimicrobial peptides (AMPs) are the primary factors of innate immunity and are the frontline of biological defense mechanisms against infection. Most AMPs are positively charged and are thought to exhibit microbicidal activity through a membrane-disrupting mechanism due to their interaction with negatively charged microbial membranes. A number of AMPs hold promise as new drugs owing to their potent bactericidal activity and because they are often refractory to the development of drug resistance. Cryptdins (Crps) are a type of AMP, also known as α-defensins, found in mouse intestinal Paneth cells, comprising six isoforms containing three sets of disulfide bonds. It has been reported that Crps contribute to the antibacterial barrier function of the small intestinal mucosa, and the selective activity of Crps may be related to the composition of the intestinal microbiota in vivo and homeostasis of the entire intestine. Furthermore, low Crp levels are thought to be closely related to dysbiosis, which is an abnormality of the intestinal microflora, and the various diseases it induces. Although Crp4 is actively being investigated, there have been few studies to date on the other Crp isoforms. The level of gene expression of different Crps in various positions in the small intestine differs, and their dissimilar characteristics indicate that different isoforms appear to have specific roles in the small intestine. Based on these backgrounds, it is very meaningful to better understand the Crp family. A better understanding of Crps requires them to be produced in a more efficient manner.

In chapter 1, I produced large amounts of most of the Crps by a novel strategy to promote inclusion body formation. In previous study, co-expression of Crp4 with the aggregation-prone protein human α-lactalbumin (HLA) was used to promote the formation of stable inclusion bodies in order to avoid the degradation of Crp4 during recombinant expression in *Escherichia coli*. Using this method, the production of Crp4

and Crp6 by the BL21 strain was effective, but the expression of other Crp isoforms was not as efficient. I considered two possible reasons why this co-expression system did not result in enhanced expression. First, when ribosomes synthesized the different Crp isoforms, the synthesis levels were different, leading to significant differences in the final amount produced. The second possibility is that there was a difference in the efficiency of inclusion body formation, even though there was not much difference in the level of ribosome synthesis for each peptide. Therefore, I first verified the amount of each Crp isoform synthesized by ribosomes using the reconstituted cell-free expression system. The results of a cell-free system study showed that except for Crp5, the expression levels of Crp1, Crp2, and Crp3 were comparable to those of Crp4 and Crp6. This suggests that the reason why low levels of insoluble granules were previously obtained with Crp1, Crp2, and Crp3 in the co-expression system with HLA in *E. coli* may be due to a limitation of the efficiency of their formation once synthesized, while for Crp5, the actual amount synthesized by the ribosomes may be limiting. Based on these results, I sought to promote the formation of insoluble granules by forming non-natural disulfide cross-links between HLA and Crps using Origami B, strain which is an expression host with an oxidative internal environment. As expected, using the Origami B strain greatly improved the expression levels of Crp1, Crp2, and Crp3. Subsequently, Crps and HLA were successfully separated by solubilizing inclusion bodies in a solubilization buffer with the addition of reducing agents and urea, and cation exchange chromatography. Refolding was performed by dialysis, then the product obtained after dialysis could be purified by reverse-phase HPLC. Each purified Crp isoform could be separated into two or three peaks, which is thought to be due to modification of the N-terminal methionine by a formyl group. Then I used acid hydrolysis to deformylate Crps with N-terminal formyl group. After exploring the

conditions, 0.6 M hydrochloric acid was considered as the optimum condition. The proportion of successful deformylation for each Crp isoform exceeded 70%. Deformylation resulted in a significant increase in the production of each Crp isoform, with yields reaching at least 3 mg/L of medium.

In Chapter 2, I studied the secondary structure and antibacterial activity of Crps prepared in the previous chapter. First, to obtain information on the steric structures of the Crps, CD spectra were measured under different conditions. In order to investigate reduced Crps, which have recently attracted attention for their activity in vivo, I also prepared Crps completely reduced with DTT. CD spectra were measured in 10mM PBS, highly hydrophobic (40% TFE) and membrane-mimetic (10 mM SDS) environments, fully reduced Crps, compared to the spectrum in 10mM PBS, showed a very large structural change, but for the Crps prepared in the previous chapter, no significant changes in the spectra were observed. This suggests that all prepared Crps had a stable secondary structure due to disulfide cross-linking and that their steric structures were stable in various environments. The bactericidal activity of Crps against Gram-positive bacteria (*Staphylococcus aureus* and *Listeria monocytogenes*) and Gram-negative bacteria (*E. coli* and *Salmonella enterica*) was analyzed. Crp4 exhibited the strongest antimicrobial activity against Gram-negative bacteria, followed by Crp3 and Crp2. Crp1 and Crp6 exhibited the weakest activities. However, Crp4 exhibited very low activity against Gram-positive bacteria, but the other four Crps all exhibited very strong bactericidal activity. These trends clearly indicate that each Crp isoform has a very different antimicrobial spectrum.

In this study, I established a novel and efficient method for the production of the cryptdin family of cysteine-containing antimicrobial peptides. Additionally, I found that there were notable differences in the antibacterial activities of the various Crp family

members. The expression system established in this study is expected to provide new insights regarding the mechanisms underlying the different antibacterial activities of the Crp family of peptides.

Chapter 1:

Production of cryptdin family peptides by a novel strategy that promotes inclusion body formation

1.1 Introduction

Antimicrobial peptides (AMPs) are the primary factors of innate immunity and are the frontline of biological defense mechanisms against infection (Boman HG, 1995). Antimicrobial peptides exhibit antimicrobial action, from a low concentration against Gram-negative bacteria to Gram-positive bacteria, fungi, yeast, spirochetes, protozoa, and ultimately viruses (Guaní-Guerra E et al., 2010; Selsted ME et al., 2005). Most AMPs are positively charged (Mahlapuu M et al., 2016; Bosch TCG et al., 2021) and are thought to exhibit microbicidal activity through a membrane-disrupting mechanism due to their interaction with negatively charged microbial membranes. However, the detailed mechanisms of membrane destruction and other such phenomena remain largely unknown. Recently, the emergence of antibiotic-resistant bacteria has become a limitation in the use of antibiotics (Li B et al., 2018). AMPs have attracted considerable attention owing to their potent activity and unique antibacterial mechanisms (Lei J et al., 2019; Li T et al., 2019; Tripathi S et al., 2013).

Cryptdins (Crps) are a type of AMP, also known as α-defensins, found in mouse intestinal Paneth cells (Ouellette AJ et al., 1989). It has been reported that Crps contribute to the antibacterial barrier function of the small intestinal mucosa, and the selective activity of Crps may be related to the composition of the intestinal microbiota *in vivo* and homeostasis of the entire intestine (Masuda K et al., 2011; Selsted ME et al., 1992; Nakamura K et al., 2020). Furthermore, low Crp levels are thought to be closely related to dysbiosis, which is an abnormality of the intestinal microflora, and the various diseases it induces. Studies in mice have shown that Crohn's disease, which

is a type of inflammatory bowel disease (Shimizu Y et al., 2020), as well as graft-versus-host disease (Hayase E et al., 2017; Eriguchi Y et al., 2015), which is a harmful immune response after bone marrow transplantation, and depression caused by psychological stress (Suzuki K et al., 2021) are strongly associated with abnormalities in Crp concentration or quality. Similar to other α-defensins, Crps have a characteristic three-stranded β-sheet structure containing six cysteine residues that form three disulfide bonds between Cys1-Cys6, Cys2-Cys4, and Cys3-Cys5 (Ouellette AJ et al., 1992). There are six different isoforms of Crp (Fig. 1-1, Table 1-1) (Ouellette AJ et al., 1994), and most studies to date have been conducted on Crp4 (Rosengren KJ et al., 2006; Masuda K et al., 2011; Sato Y et al, 2022) and only a few on other Crps. The level of gene expression of different Crps in various positions in the small intestine differs, and their dissimilar characteristics indicate that different isoforms appear to have specific roles in the small intestine (Ouellette AJ et al., 1994; Preet S et al., 2011; Lencer WI et al., 1997; Inoue R et al., 2008). A better understanding of Crps requires them to be produced in a more efficient manner.

Recombinant expression is an economical method of protein production. However, recombinant production of AMPs has been hindered because of their tendency to undergo degradation by host proteases and/or because they are toxic to the host cells (Schreiber C et al., 2017; Hu F et al., 2010). The formation of inclusion bodies is known to be a method that can prevent these undesirable events from taking place (Rao X et al., 2005; Lee JH et al., 1998; Feng XJ et al., 2014; Hoffmann D et al., 2018). However, because of the high solubility of AMPs as a result of their high positive charge, simple

expression often makes it difficult to form inclusion bodies of them. To solve this limitation, I developed a method in which AMPs are successfully co-expressed as inclusion bodies with aggregation-prone and negatively charged human α-lactalbumin (HLA) (Tomisawa S et al., 2013; Kuddus MR et al., 2017; Tomisawa S et al., 2015). The electrostatic and hydrophobic interactions between AMPs and HLA are presumably responsible for the enhanced inclusion body formation. Using this expression system, we have previously succeeded in mass expression of Crp4, but the application of this method to other Crp isoforms has not been investigated to date.

Thus, this study examined the application of this method to the production of Crp isoforms other than Crp4. Interestingly, despite the homology between Crp isoforms, there were large differences in their expression levels. I sought to increase their expression levels by examining the causes of this difference and by investigating new methods to promote inclusion body formation.

1.2 Materials and Methods

Strains, Vectors, and Reagents

DNA cloning was performed using the *E. coli* DH5α strain and pCOLADuet1 and pET-16b plasmid. *E. coli* BL21(DE3) and *E. coli* Origami™ B(DE3) were used for expression analysis. All *E. coli* strains and vectors were obtained from Novagen. DNA extractions were performed with a FastGene® Plasmid Mini Kit (NIPPON Genetics Co., Ltd.), and the FastDigest® restriction enzymes *Xho* I, *Nde* I, *Nco* I, *Bam*H I, and *Bgl* II were purchased from Thermo Fisher Scientific.

Plasmid construction

In this study, because co-expression was required, the DNA sequences of the partner protein HLA and the target Crps were inserted into the pCOLADute1 plasmid (Fig. 1-2a). In addition to the pCOLADuet vector, which is kanamycin-resistant and has a ColA replication origin, similar insertions were made into the pET-16b plasmid, which is ampicillin-resistant and has a ColE1 replication origin (Fig. 1-2b). Thus, the vectors containing the HLA and Crps genes can be expressed in the kanamycin-resistant Origami™ B strain. The 372 bp fragment encoding the partner protein HLA was inserted into the *Nco* I and *Bam*H I restriction sites of the vector pCOLA-Duet1, and the 99–108 bp fragments encoding the target protein Crp isoforms were inserted into the *Nde* I and *Xho* I restriction sites. *E. coli* DH5α were transformed with the plasmids, and positive transformants were screened on lysogeny broth (LB) plates and confirmed using a DNA sequencer (Applied Biosystems 3130 Genetic Analyzer). The resulting

pCOLA-Duet1 plasmids were digested with the endonucleases *Bgl* II and *Xho* I, and the fragments were inserted into pET-16b. After confirmation by DNA sequencing, the expression strains were transformed with the vectors.

Expression of Crps in the *E. coli* expression system

The *E. coli* BL21(DE3) and Origami™ B(DE3) strains transformed with the plasmid pET-16b-HLA-Crps were inoculated into 5 mL of LB medium containing 50 μg/mL ampicillin and incubated at 37°C with shaking at 180 rpm until the absorbance at 600 nm reached 1.0. Expression was induced by the addition of IPTG, and the bacterial liquid was subjected to shaking at 180 rpm for 4 h. The cells were collected by centrifugation at 10,000 rpm for 3 min and washed with disruption buffer (20 mM Tris-HCl (pH 8) and 1 mM EDTA). One milliliter of the medium was resuspended in 100 μL of buffer and disrupted with a sonicator (Misonix™ Microson™ Ultrasonic Cell Disruptor XL2000) on ice. The mixture was centrifuged at 10,000 rpm for 3 min. The amount of protein in the obtained supernatant and pellet was confirmed by Tricine-SDS-PAGE (n=3 for each).

Expression in PURE system

The plasmid pET-16b-HLA-Crps was added to the PURE system (PURExpress2.0) at a concentration of 2 ng/μL. The entire reaction was carried out in an RNase-free environment. The cells were incubated at 37°C for 4 h. The amount of protein in the reaction system was confirmed by Tricine-SDS-PAGE (n=3 for each).

Large-scale expression of Crps for purification

Origami™ B transformed with plasmid pET-16b-HLA-Crps was inoculated into 50 mL of LB medium containing 50 μg/mL ampicillin and incubated overnight at 30°C and 180 rpm. The mixture was centrifuged at 6000 rpm for 5 min and resuspended in 500 mL of LB medium containing 50 μg/mL ampicillin. The culture was incubated at 37°C with shaking at 120 rpm. Once the absorbance at 600 nm reached 1.0, 1 mM IPTG was added to induce protein expression. After culturing at 30°C with shaking at 120 rpm for 6 h, the bacterial solution was centrifuged at 6000 rpm for 10 min, and the bacterial cells were washed with disruption buffer and stored.

Purification and analysis of Crps

The obtained bacterial cells were resuspended in fragmentation buffer (20mM Tris-HCl (pH8.0), 1mM EDTA), crushed in an ultrasonic crusher (Insonator 201M, KUBOTA) at 180W for 30 min, and centrifuged at 4300 × g for 20 min to obtain a precipitate containing inclusion bodies. The pellet was resuspended in a solubilization buffer (50 mM glycine-NaOH (pH8.5), 3 mM EDTA, and 6 M urea, final pH 9.0) and incubated at 24°C with shaking at 180 rpm for 1 h so that almost all of the inclusion bodies were dissolved. After centrifugation at 7000 × g for 20 min, the supernatant was loaded onto an SP Sepharose® FAST FLOW cation exchange column (Cytiva™) equilibrated with 50 mM glycine-NaOH (pH 8.5), 3 mM EDTA, 6 M urea, and 20 mM β-mercaptoethanol, final pH 9.0. The bound Crps were eluted using a linear gradient of

0–1 M NaCl buffer. The fractions containing Crps were refolded twice at 4°C using refolding buffer containing 50 mM glycine-NaOH (pH8.5), 2 M urea, 3 mM reduced glutathione, 0.3 mM oxidized glutathione, and 10% glycerol, final pH 9.0, for approximately 12 h each time, after which 0.1% acetic acid was dialyzed overnight to remove other compounds in the system. The dialyzed Crps were purified by RP-HPLC using a COSMOSIL® Protein-R column (Nacalai Tesque). Elution was performed using a linear gradient of 0–50% acetonitrile and 0.1% TFA. Yields were calculated based on the absorbance at 280 nm. The molecular weights of the eluted Crps were determined by MALDI-TOF-MS (autoflex™ speed, Bruker).

Deformylation

We added 0, 7.5, 15, and 50 μL of 6 M hydrochloric acid to 100 μL of formyl-Crp6 at a concentration of approximately 1 mg/mL, and ddH_2O was added to bring the total volume to 150 μL. The final concentration of hydrochloric acid in each group was 0, 0.3, 0.6, and 2 M. A 100 μL aliquot of each of the other formyl-Crps at a concentration of approximately 1 mg/mL was deamidated with 0.6 M hydrochloric acid.

After incubation at 37°C for more than 20 h, the reaction was terminated by the addition of 850 μL ddH_2O, the pH was adjusted to 2–3 using NaOH, and RP-HPLC was used to analyze the amount of each component.

1.3 Results and Discussion

Co-expression of the various Crp isoforms with aggregation-prone proteins

When various Crp isoforms were expressed using the pET overexpression system with *E. coli* Bl21 strain and T7 promoter-driven gene expression, little Crp expression was observed after IPTG induction (Fig. 1-3). It is thought that AMPs which require disulfide cross-linking to form their stable conformation are often degraded because of their instability when expressed in a reducing intracellular environment, thus resulting in a low level of production. Therefore, I tested our previously developed expression system (Tomisawa S et al., 2013; Kuddus MR et al., 2017; Tomisawa S et al., 2015). That promotes inclusion body formation by co-expression of AMPs with HLA, which has a high propensity for aggregation (Fig. 1-4a). Tricine-SDS-PAGE of overexpressed inclusion bodies showed a clear increase in Crp4 expression, consistent with our previous results, as well as an increase in Crp6 expression (Fig. 1-4b, c). However, although the expression was increased compared with the expression of the peptides alone, the effect was minor for Crp1 and very minor for Crp2, Crp3, and Crp5.

Two main reasons come to mind why this co-expression system did not result in enhanced expression. First, when ribosomes synthesized the different Crp isoforms, the synthesis levels were different, leading to significant differences in the final amount produced. The second possibility is that there was a difference in the efficiency of inclusion body formation, even though there was not much difference in the level of ribosome synthesis for each peptide.

Confirmation of the amount synthesized by ribosomes using a cell-free synthesis system

Therefore, I first verified the amount of each Crp isoform synthesized by ribosomes using the PURE cell-free expression system (Shimizu Y et al., 2005; Shimizu Y et al., 2001; Shimizu Y et al., 2010). Because the PURE system is a fully reconstituted cell-free system using *E. coli* ribosomes, it allows comparison of the synthesis of each Crp isoform by ribosomes in the absence of the effects of intracellular protease degradation (Hino M et al., 2008; El-Baky NA et al., 2021; Spirin AS et al., 2004). The plasmid containing the genes coding for HLA and Crp was added to the expression system and allowed to react for 4 h, and the obtained product was confirmed by tricine-SDS-PAGE (Fig. 1-5). With the exception of Crp5, the expression levels of Crp1, Crp2, and Crp3 were comparable to those of Crp4 and Crp6. This suggests that the reason why low levels of insoluble granules were previously obtained with Crp1, Crp2, and Crp3 in the co-expression system with HLA in *E. coli* may be due to a limitation of the efficiency of their formation once synthesized, while for Crp5, the actual amount synthesized by the ribosomes may be limiting. As shown in Table 1-2, Crp2, Crp3, and Crp6 have extremely high sequence homology compared with Crp1, whereas Crp5 has low homology. Therefore, the low expression of Crp5 by ribosomes compared with the other Crp isoforms may be sequence-specific. It is possible that the low production of Crp5 was not only due to the abundance of tRNA (Ikemura T, 1985), but also its DNA sequence, which resulted in the structure of its mRNA not being conducive to translation by the ribosomes of *E. coli* (Kozak M, 2005). The folding free energy of

mRNA is responsible for its secondary structure formation and stability. It is known that the formation of secondary structure near the ribosome binding site, the Shine-Dalgarno (SD) sequence, of mRNA interferes with ribosome binding and reduces translation efficiency (De Smit MH et al., 1990; Jacques N et al., 1990; Bhattacharyya S et al., 2018). Thus, preventing the formation of secondary structure of such mRNAs may increase the efficiency of Crp5 synthesis by the ribosome and improve production efficiency. Silent mutations using synonymous codons that do not alter the amino acid sequence may be effective for this purpose. For example, it has been reported that by the substitution of synonymous codons, reducing the GC rate, increasing the mRNA folding free energy at the 5'-terminal ends, and thus making the secondary structure of mRNA more unstable, can lead to an increase in protein expression (Dewi KS et al., 2020; Kudla G et al., 2009). Such improved peptide synthesis by the ribosome is expected to be directly related to the increased production of Crp5. In contrast, it is unclear why Crp1, Crp2, and Crp3, which are highly homologous to Crp6 and are not limited by ribosomal synthesis, were not efficient in terms of inclusion body formation. Previous studies have shown that electrostatic and hydrophobic interactions play an important role in efficient inclusion body formation in our co-expression system. However, I could not find any trend in Crp family isoelectric points or GRAVY scores (Table 1-1) that might explain the success or failure of inclusion body formation. Various culture conditions, such as the type of medium, the culture temperature, and IPTG induction conditions were examined with the aim of achieving more efficient

inclusion body formation, but unfortunately, no improvement in the expression was observed (data not shown).

Enhancement of inclusion body formation by disulfide cross-link formation

Based on these results, I sought to promote the formation of insoluble granules by forming non-natural disulfide cross-links between the partner protein and the Crps (Fig. 1-6a). The cellular redox state of normal *E. coli*, such as BL21, is reducing, which generally precludes disulfide cross-link formation. In contrast, the Origami™ B strain is an expression host developed to obtain proteins with natural disulfide bond formation in the cell by the introduction of mutations in *trxB* and *gor* (Prinz WA et al., 1997; Bessette PH et al., 1999), thereby creating an oxidizing redox state in the cells. Therefore, in this study, I sought to promote the formation of non-natural disulfide cross-links, contrary to the original purpose of using the Origami™ strain. As expected, using the Origami™ B strain greatly improved the expression levels of Crp1, Crp2, and Crp3 (Fig. 1-6b, c). There was not, however, a significant increase in Crp5 expression, suggesting that, as expected, the amount of synthesis by the ribosomes is limiting for Crp5.

The Origami™ strain is a frequently used host for the efficient formation of wild-type disulfide bonds and has been used with great success (Soheili S et al., 2020; Safary A et al., 2016; Long X et al., 2015). However, to the best of our knowledge, this is the first report of the use of unnatural-type disulfide bond formation in cells to promote inclusion body formation. This approach has great potential as a versatile technique for

the efficient formation of inclusion bodies of peptides that are otherwise prone to degradation in the cell.

Large-scale overexpression and purification of Crps

Large-scale culture and purification conditions were investigated to obtain abundant quantities of individual Crp peptide isoforms. After assessing various incubation conditions, the optimal induction condition was found to be 30°C for 6 hours (Slouka C et al., 2018; Gutiérrez-González M et al., 2019). The inclusion complexes containing Crp and HLA were separated by solubilizing them with a denaturing agent containing a reducing agent to cleave the disulfide bonds between them, followed by purification using cation exchange chromatography (Fig. 1-7). Tricine-SDS-PAGE showed that each main peak contained a Crp isoform, but the amount of Crp5 was insufficient to allow further experiments to be conducted (data not shown). One method for forming an inclusion body of the peptide is to fuse the peptide to a highly insoluble protein, such as KSI, as used with the pET31 expression vector (Rodríguez V et al., 2014; Sun YL et al., 2010). However, this method requires chemical cleavage with CNBr, or another chemical cleavage must be performed, to separate the peptide from the fusion protein. Such cleavage methods may result in poor selectivity and undesirable side reactions. Our method using co-expression is superior in the sense that it can efficiently separate the partner HLA from the target peptide using a simple reducing agent containing a denaturing agent.

Subsequently, refolding was performed by removal of the urea, β-mercaptoethanol, and salts by dialysis. With the exception of Crp5, the product obtained after dialysis could be purified by reverse-phase HPLC. Each purified Crp isoform could thereby be separated into two or three peaks, as shown in Fig. 1-8. The products were analyzed using MALDI-TOF mass spectrometry, and the results obtained are indicated above the peaks in Fig. 1-8. Among these, the molecular weight of peak (1) of each Crp isoform was approximately 6 Da smaller than that of its fully reduced peptide (Table 1-1), indicating that Crps that refolded successfully by forming three disulfide bonds were obtained using this expression purification system. In addition, peak (2) had a molecular weight 28 Da larger than that of peak (1), which is thought to be due to modification of the N-terminal methionine by a formyl group (Warren WC et al., 1996; Piatkov KI et al., 2015). For Crp4, a peak (*) with a smaller molecular weight was observed earlier than peak (1). This is because the side chain length of glycine, which is the amino acid following the N-terminal methionine of Crp4, is sufficiently short for the N-terminal methionine to be cleaved by methionine aminopeptidase (Hirel PH et al., 1989). The yields of the various products are listed in Table 1-3.

The residual formyl groups on the N-terminal methionine were further investigated. For comparison, the results of Crp6 expression using the BL21 strain showed that the product also contained Crp6 with N-terminal methionine formylation (Fig. 1-9); however, the amount was clearly lower than that obtained using the Origami™ B strain. Normally, the N-terminal formyl group is removed by the intracellular peptide deformylase (PDF) (Piatkov KI et al., 2015; Bögeholz LAK et al., 2021). However, it

has been reported that when excessive amounts of recombinant proteins are expressed, the degradation efficiency of PDF is reduced, and the products contain proteins with formylmethionine (Warren WC et al., 1996). Furthermore, it has been reported that nascent peptides with less than 50 amino acids readily retain the formyl group (Housman D et al., 1972). Also, the activity of PDF is affected by certain metal ions in *E. coli*, such as Fe^{2+} (Rajagopalan PTR et al., 1997; Ragusa S et al., 1998; Rajagopalan PTR et al., 1998). The present results suggest that the oxidative intracellular environment of the Origami™ B strain may have affected the Fe^{2+} concentration, decreased PDF activity, and hence resulted in an increase in the content of formylated Crp in the product.

Attempts to increase the yield by chemical deformylation

To further increase the yield of Crps, I first investigated the conditions for deformylation by the acidic hydrolysis method (Elson NA et al., 1974; Chan SJ et al., 1981) using purified formylated Crp6. The results of the analysis using RP-HPLC after reaction with various concentrations of HCl for more than 20 h are shown in Fig. 1-10a. After acid hydrolysis, three main peaks were observed. The amount of Crp6 that was successfully deformylated (Peak 1) from the formylated Crp6 (Peak 2) increased in an HCl concentration-dependent manner, but the byproducts (peaks indicated by *), which were further hydrolyzed between the aspartic acid at the fourth position and the leucine at the fifth position, also increased. Among these, more than 70% of the formyl-Crp6 was successfully deformylated into Crp6 after exposure to 0.6 M hydrochloric acid, and

the proportion of byproducts was not high (Fig. 1-10b). Therefore, considering the proportion of deformylation and byproducts, hydrolysis with 0.6 M HCl was determined to be the optimal condition, and other Crps were also treated with 0.6 M HCl (Fig. 1-11), and their component ratios are listed in Table 1-4. The proportion of successful deformylation for each Crp isoform exceeded 80%.

The yields of successfully deformylated Crps and the final Crp isoform yields obtained were calculated and are presented in Table 1-3. Chemical deformylation resulted in a significant increase in the production of each Crp isoform, with yields reaching at least 3 mg/L of medium.

1.4 References

Boman HG. Peptide antibiotics and their role in innate immunity. Annu Rev Immunol. 1995;13:61–92. https://doi.org/10.1146/annurev.iy.13.040195.000425

Guaní-Guerra E, Santos-Mendoza T, Lugo-Reyes SO, Terán LM. Antimicrobial peptides: General overview and clinical implications in human health and disease. Clin Immunol. 2010. Elsevier Inc.;135:1–11. http://doi.org/10.1016/j.clim.2009.12.004

Selsted ME, Ouellette AJ. Mammalian defensins in the antimicrobial immune response. Nat Immunol. 2005;6:551–7. https://doi.org/10.1038/ni1206

Mahlapuu M, Håkansson J, Ringstad L, Björn C. Antimicrobial peptides: An emerging category of therapeutic agents. Front Cell Infect Microbiol. 2016;6:194. https://doi.org/10.3389/fcimb.2016.00194

Bosch TCG, Zasloff M. Antimicrobial peptides—Or how our ancestors learned to control the microbiome. mBio. 2021;12:e0184721. https://doi.org/10.1128/mBio.01847-21

Li B, Webster TJ. Bacteria antibiotic resistance: New challenges and opportunities for implant-associated orthopedic infections. J Orthop Res. 2018;36:22–32. https://doi.org/10.1002/jor.23656

Lei J, Sun LC, Huang S, Zhu C, Li P, He J, et al. The antimicrobial peptides and their potential clinical applications. Am J Transl Res. 2019;11:3919–31

Li T, Liu Q, Wang D, Li J. Characterization and antimicrobial mechanism of CF-14, a new antimicrobial peptide from the epidermal mucus of catfish. Fish Shellfish Immunol. 2019. Elsevier;92:881–8. https://doi.org/10.1016/j.fsi.2019.07.015

Tripathi S, Tecle T, Verma A, Crouch E, White M, Hartshorn KL. The human cathelicidin LL-37 inhibits influenza A viruses through a mechanism distinct from that of surfactant protein D or defensins. J Gen Virol. 2013;94:40–9. https://doi.org/10.1099/vir.0.045013-0

Ouellette AJ, Greco RM, James M, Frederick D, Naftilan J, Fallon JT. Developmental regulation of cryptdin, a corticostatin/defensin precursor mRNA in mouse small intestinal crypt epithelium. J Cell Biol. 1989;108:1687–95. https://doi.org/10.1083/jcb.108.5.1687

Masuda K, Nakamura K, Yoshioka S, Fukaya R, Sakai N, Ayabe T. Regulation of microbiota by antimicrobial peptides in the gut. Adv Oto-Rhino-Laryngol. 2011;72:97–9. https://www.karger.com/DOI/10.1159/000324625. https://doi.org/10.1159/000324625

Selsted ME, Miller SI, Henschen AH, Ouellette AJ. Enteric defensins: Antibiotic peptide components of intestinal host defense. J Cell Biol. 1992;118:929–36. https://doi.org/10.1083/jcb.118.4.929

Nakamura K, Yokoi Y, Fukaya R, Ohira S, Shinozaki R, Nishida T, et al. Expression and localization of Paneth cells and their α-defensins in the small intestine of adult mouse. Front Immunol. 2020;11:570296. https://doi.org/10.3389/fimmu.2020.570296

Shimizu Y, Nakamura K, Yoshii A, Yokoi Y, Kikuchi M, Shinozaki R, et al. Paneth cell α-defensin misfolding correlates with dysbiosis and ileitis in Crohn's disease model mice. Life Sci Alliance. 2020;3:1–15. https://doi.org/10.26508/lsa.201900592

Hayase E, Hashimoto D, Nakamura K, Noizat C, Ogasawara R, Takahashi S, et al. R-Spondin1 expands Paneth cells and prevents dysbiosis induced by graft-versus-host disease. J Exp Med. 2017;214:3507–18. https://doi.org/10.1084/jem.20170418

Eriguchi Y, Nakamura K, Hashimoto D, Shimoda S, Shimono N, Akashi K, et al. Decreased secretion of Paneth cell α-defensins in graft-versus-host disease. Transpl Infect Dis. 2015;17:702–6. https://doi.org/10.1111/tid.12423

Suzuki K, Nakamura K, Shimizu Y, Yokoi Y, Ohira S, Hagiwara M, et al. Decrease of α-defensin impairs intestinal metabolite homeostasis via dysbiosis in mouse chronic social defeat stress model. Sci Rep. 2021. UK: Nature Publishing Group;11:9915. https://doi.org/10.1038/s41598-021-89308-y

Ouellette AJ, Miller SI, Henschen AH, Selsted ME. Purification and primary structure of murine cryptdin-1, a Paneth cell defensin. FEBS Lett. 1992;304:146–8. https://doi.org/10.1016/0014-5793(92)80606-h

Ouellette AJ, Hsieh MM, Nosek MT, Cano-Gauci DF, Huttner KM, Buick RN, et al. Mouse Paneth cell defensins: Primary structures and antibacterial activities of numerous cryptdin isoforms. Infect Immun. 1994;62:5040–7. https://doi.org/10.1128/iai.62.11.5040-5047.1994

Rosengren KJ, Daly NL, Fornander LM, Jönsson LMH, Shirafuji Y, Qu X, et al. Structural and functional characterization of the conserved salt bridge in mammalian

paneth cell α-defensins: Solution structures of mouse cryptdin-4 and (E15D)-cryptdin-4. J Biol Chem. 2006;281:28068–78. https://doi.org/10.1074/jbc.M604992200

Masuda K, Sakai N, Nakamura K, Yoshioka S, Ayabe T. Bactericidal activity of mouse α-defensin cryptdin-4 predominantly affects noncommensal bacteria. J Innate Immun. 2011;3:315–26. https://doi.org/10.1159/000322037

Sato Y, Wang Y, Song Y, Geng W, Yan S, Nakamura K, et al. Potent bactericidal activity of reduced cryptdin-4 derived from its hydrophobicity and mediated by bacterial membrane disruption. Amino Acids. 2022;54:289–97. https://doi.org/10.1007/s00726-021-03115-3

Preet S, Bharati S, Shukla G, Koul A, Rishi P. Evaluation of amoebicidal potential of paneth cell cryptdin-2 against Entamoeba histolytica. PLOS Negl Trop Dis. 2011;5:e1386. https://doi.org/10.1371/journal.pntd.0001386

Lencer WI, Cheung G, Strohmeier GR, Currie MG, Ouellette AJ, Selsted ME, et al. Induction of epithelial chloride secretion by channel-forming cryptdins 2 and 3. Proc Natl Acad Sci U S A. 1997;94:8585–9. https://doi.org/10.1073/pnas.94.16.8585

Inoue R, Tsuruta T, Nojima I, Nakayama K, Tsukahara T, Yajima T. Postnatal changes in the expression of genes for cryptdins 1–6 and the role of luminal bacteria in cryptdin gene expression in mouse small intestine. FEMS Immunol Med Microbiol. 2008;52:407–16. https://doi.org/10.1111/j.1574-695X.2008.00390.x

Schreiber C, Müller H, Birrenbach O, Klein M, Heerd D, Weidner T, et al. A high-throughput expression screening platform to optimize the production of antimicrobial

peptides. Microb Cell Factories. 2017. BioMed Central;16:29. https://doi.org/10.1186/s12934-017-0637-5

Hu F, Ke T, Li X, Mao PH, Jin X, Hui FL, et al. Expression and purification of an antimicrobial peptide by fusion with elastin-like polypeptides in Escherichia coli. Appl Biochem Biotechnol. 2010;160:2377–87. https://doi.org/10.1007/s12010-009-8850-2

Rao X, Hu J, Li S, Jin X, Zhang C, Cong Y, et al. Design and expression of peptide antibiotic hPAB-β as tandem multimers in Escherichia coli. Peptides. 2005;26:721–9. https://doi.org/10.1016/j.peptides.2004.12.016

Lee JH, Minn I, Park CB, Kim SC. Acidic peptide-mediated expression of the antimicrobial peptide buforin II as tandem repeats in Escherichia coli. Protein Expr Purif. 1998;12:53–60. https://doi.org/10.1006/prep.1997.0814

Feng XJ, Xing LW, Liu D, Song XY, Liu CL, Li J, et al. Design and high-level expression of a hybrid antimicrobial peptide LF15-CA8 in Escherichia coli. J Ind Microbiol Biotechnol. 2014;41:527–34. https://doi.org/10.1007/s10295-013-1382-3

Hoffmann D, Ebrahimi M, Gerlach D, Salzig D, Czermak P. Reassessment of inclusion body-based production as a versatile opportunity for difficult-to-express recombinant proteins. Crit Rev Biotechnol. 2018. Taylor & Francis;38:729–44. https://doi.org/10.1080/07388551.2017.1398134

Tomisawa S, Hojo E, Umetsu Y, Ohki S, Kato Y, Miyazawa M, et al. Overexpression of an antimicrobial peptide derived from C. elegans using an

aggregation-prone protein co-expression system. AMB Express. 2013;3:1 https://doi.org/10.1186/2191-0855-3-45

Kuddus MR, Yamano M, Rumi F, Kikukawa T, Demura M, Aizawa T. Enhanced expression of cysteine-rich antimicrobial peptide snakin-1 in Escherichia coli using an aggregation-prone protein co-expression system. Biotechnol Prog. 2017;33:1520–8. https://doi.org/10.1002/btpr.2508

Tomisawa S, Sato Y, Kamiya M, Kumaki Y, Kikukawa T, Kawano K, et al. Efficient production of a correctly folded mouse α-defensin, cryptdin-4, by refolding during inclusion body solubilization. Protein Expr Purif. 2015. Elsevier Inc.;112:21–8. http://doi.org/10.1016/j.pep.2015.04.007

Shimizu Y, Kanamori T, Ueda T. Protein synthesis by pure translation systems. Methods. 2005;36:299–304.

Shimizu Y, Inoue A, Tomari Y, Suzuki T, Yokogawa T, Nishikawa K, et al. Supplemental Material for "Cell-free translation reconstituted with purified components." Nat Biotechnol. 2001;19:751–5.

Shimizu Y, Ueda T. PURE Technology. In: Endo Y, Takai K, Ueda T, editors. Cell-Free Protein Prod Methods Protoc. Totowa, NJ: Humana Press; 2010. p. 11–21. https://doi.org/10.1007/978-1-60327-331-2_2

Hino M, Kataoka M, Kajimoto K, Yamamoto T, Kido JI, Shinohara Y, et al. Efficiency of cell-free protein synthesis based on a crude cell extract from Escherichia coli, wheat germ, and rabbit reticulocytes. J Biotechnol. 2008;133:183–9.

El-Baky NA, Elkhawaga MA, Abdelkhalek ES, Sharaf MM, Redwan EM, Kholef HR. De novo expression and antibacterial potential of four lactoferricin peptides in cell-free protein synthesis system. Biotechnol Rep (Amst). 2021. Elsevier BV;29:e00583. https://doi.org/10.1016/j.btre.2020.e00583

Spirin AS. High-throughput cell-free systems for synthesis of functionally active proteins. Trends Biotechnol. 2004;22:538–45. https://doi.org/10.1016/j.tibtech.2004.08.012

Ikemura T. Codon usage and tRNA content in unicellular and multicellular organisms. Mol Biol Evol. 1985;2:13–34. https://doi.org/10.1093/oxfordjournals.molbev.a040335

Kozak M. Regulation of translation via mRNA structure in prokaryotes and eukaryotes. Gene. 2005;361:13–37. https://doi.org/10.1016/j.gene.2005.06.037

De Smit MH, Van Duin J. Secondary structure of the ribosome binding site determines translational efficiency: A quantitative analysis. Proc Natl Acad Sci U S A. 1990;87:7668–72. https://doi.org/10.1073/pnas.87.19.7668

Jacques N, Dreyfus M. Translation initiation in Escherichia coli: Old and new questions. Mol Microbiol. 1990;4:1063–7. https://doi.org/10.1111/j.1365-2958.1990.tb00679.x

Bhattacharyya S, Jacobs WM, Adkar B V., Yan J, Zhang W, Shakhnovich EI. Accessibility of the Shine-Dalgarno Sequence Dictates N-Terminal Codon Bias in E. coli. Mol Cell. 2018;70:894-905.e5. https://doi.org/10.1016/j.molcel.2018.05.008

Dewi KS, Fuad AM. Improving the expression of human granulocyte colony stimulating factor in Escherichia coli by reducing the GC-content and increasing mRNA folding free energy at 5′-terminal end. Adv Pharm Bull. 2020;10:610–6. https://doi.org/10.34172/apb.2020.073

Kudla G, Murray AW, Tollervey D, Plotkin JB. Coding-sequence determinants of gene expression in Escherichia coli. Science. 2009;324:255–8. https://doi.org/10.1126/science.1170160

Prinz WA, Åslund F, Holmgren A, Beckwith J. The role of the thioredoxin and glutaredoxin pathways in reducing protein disulfide bonds in the Escherichia coli cytoplasm. J Biol Chem. 1997;272:15661–7. https://doi.org/10.1074/jbc.272.25.15661

Bessette PH, Åslund F, Beckwith J, Georgiou G. Efficient folding of proteins with multiple disulfide bonds in the Escherichia coli cytoplasm. Proc Natl Acad Sci U S A. 1999;96:13703–8. https://doi.org/10.1073/pnas.96.24.13703

Soheili S, Jahanian-Najafabadi A, Akbari V. Evaluation of soluble expression of recombinant granulocyte macrophage stimulating factor (rGM-CSF) by three different E. coli strains. Res Pharm Sci. 2020;15:218–25. https://doi.org/10.4103/1735-5362.288424

Safary A, Moniri R, Hamzeh-Mivehroud M, Dastmalchi S. A strategy for soluble overexpression and biochemical characterization of halo-thermotolerant Bacillus laccase in modified E. coli. J Biotechnol. 2016. Elsevier BV;227:56–63. http://doi.org/10.1016/j.jbiotec.2016.04.006

Long X, Gou Y, Luo M, Zhang S, Zhang H, Bai L, et al. Soluble expression, purification, and characterization of active recombinant human tissue plasminogen activator by auto-induction in E. coli. BMC Biotechnol. 2015;15:13. https://doi.org/10.1186/s12896-015-0127-y

Slouka C, Kopp J, Hutwimmer S, Strahammer M, Strohmer D, Eitenberger E, et al. Custom made inclusion bodies: Impact of classical process parameters and physiological parameters on inclusion body quality attributes. Microb Cell Factories. 2018. BioMed Central;17:148. https://doi.org/10.1186/s12934-018-0997-5

Gutiérrez-González M, Farías C, Tello S, Pérez-Etcheverry D, Romero A, Zúñiga R, et al. Optimization of culture conditions for the expression of three different insoluble proteins in Escherichia coli [Sci. rep.]. Sci Rep. 2019;9:16850. https://doi.org/10.1038/s41598-019-53200-7

Rodríguez V, Asenjo JA, Andrews BA. Design and implementation of a high yield production system for recombinant expression of peptides. Microb Cell Factories. 2014;13:65. https://doi.org/10.1186/1475-2859-13-65

Sun YL, Kuan TC, Lin YJ, Chou YC, Lin CS. Construction and expression of rabbit neutrophil peptide-1 gene in Escherichia coli. Ann Microbiol. 2010;60:329–34. https://doi.org/10.1007/s13213-010-0046-z

Warren WC, Bentle KA, Schlittler MR, Schwane AC, O'Neil JP, Bogosian G. Increased production of peptide deformylase eliminates retention of formylmethionine in bovine somatotropin overproduced in Escherichia coli. Gene. 1996;174:235–8. https://doi.org/10.1016/0378-1119(96)00086-8

Piatkov KI, Vu TTM, Hwang CS, Varshavsky A. Formyl-methionine as a degradation signal at the N-termini of bacterial proteins. Microb Cell. 2015;2:376–93. https://doi.org/10.15698/mic2015.10.231

Hirel PH, Schmitter MJ, Dessen P, Fayat G, Blanquet S. Extent of N-terminal methionine excision from Escherichia coli proteins is governed by the side-chain length of the penultimate amino acid. Proc Natl Acad Sci U S A. 1989;86:8247–51. https://doi.org/10.1073/pnas.86.21.8247

Bögeholz LAK, Mercier E, Wintermeyer W, Rodnina MV. Kinetic control of nascent protein biogenesis by peptide deformylase. Sci Rep. 2021. UK: Nature Publishing Group;11:24457. https://doi.org/10.1038/s41598-021-03969-3

Housman D, Gillespie D, Lodish HF. Removal of formyl-methionine residue from nascent bacteriophage f2 protein. J Mol Biol. 1972;65:163–6. https://doi.org/10.1016/0022-2836(72)90498-6

Rajagopalan PTR, Datta A, Pei D. Purification, characterization, and inhibition of peptide deformylase from Escherichia coli. Biochemistry. 1997;36:13910–8. https://doi.org/10.1021/bi971155v

Ragusa S, Blanquet S, Meinnel T. Control of peptide deformylase activity by metal cations. J Mol Biol. 1998;280:515–23. https://doi.org/10.1006/jmbi.1998.1883

Rajagopalan PTR, Pei D. Oxygen-mediated inactivation of peptide deformylase. J Biol Chem. Currently published by Elsevier Inc; originally published by American Society for Biochemistry and Molecular Biology. 1998;273:22305–10. http://doi.org/10.1074/jbc.273.35.22305

Elson NA, Brewer HB, Anderson WF. Hemoglobin switching in sheep and goats. 3. Cell-free initiation of sheep globin synthesis. J Biol Chem. 1974;249:5227–35. https://doi.org/10.1016/S0021-9258(19)42352-1

Chan SJ, Ackerman EJ, Quinn PS, Sigler PB, Steiner DF. Use of formylated yeast initiator Met tRNA to define the NH 2-terminal residues of rat preproinsulin and pregrowth hormone. J Biol Chem. 1981;256:3271–5. https://doi.org/10.1016/S0021-9258(19)69601-8

Table 1-1 Characteristics of cryptdins.

Crps	Mw	PI	GRAVY score	Charge*
Crp1	4253.12	9.61	-0.483	+7
Crp2	4384.32	9.86	-0.647	+8
Crp3	4411.39	9.99	-0.736	+9
Crp4	3886.55	9.86	-0.397	+8
Crp5	4339.32	9.86	0.169	+8
Crp6	4267.21	9.61	-0.339	+7

Molecular weight of fully reduced form (Mw), isoelectric point (pI), and grand average of hydropathy (GRAVY). *The charge was calculated from the following values at pH 7.4: Asp, -1; Glu, -1; Arg, +1; Lys, +1.

Table 1-2. Amino acid sequence identity and similarity of Crps.

Identity and similarity (%)	Crp1	Crp2	Crp3	Crp4	Crp5	Crp6
Crp1		91.67	91.67	39.47	55.56	94.44
Crp2	94.44		97.22	42.11	58.33	88.89
Crp3	91.67	97.22		44.74	58.33	88.89
Crp4	44.74	47.37	50.00		47.37	39.47
Crp5	66.67	69.44	69.44	55.26		55.56
Crp6	94.44	88.89	88.89	44.74	69.44	

Table 1-3. The yield of each Crp isoform.

Purification step		Yield (mg/L of culture)				
		Crp1	Crp2	Crp3	Crp4	Crp6
CIEX	Crude extract	5.0	5.2	5.3	8.5	9.1
RP-HPLC	Crps	1.5	0.95	0.92	1.9*	1.8
	Formyl-Crps	1.7	2.3	2.3	5.3	3.0
Deformylation	Crps	1.4	2.0	1.9	4.2	2.2
Total Crps		2.9	3.0	2.8	6.1*	4.0

The total yield of Crps was obtained by adding the amount of Crps after purification by RP-HPLC to the amount of Crps after deformylation.

*Crp4 represents the sum of the total amounts of Crp4 with and without methionine.

Table 1-4. Quantitative results of the amount of deformylation of Crps.

Crps	Proportion (%)			
	Before defomylation	After deformyltion		
	Formyl-Crps	Formyl-Crps	**Crps**	By-product
Crp1	100	10	**83**	2
Crp2	100	11	**85**	2
Crp3	100	11	**84**	2
Crp4	100	10	**80**	5
Crp6	100	8	**73**	16

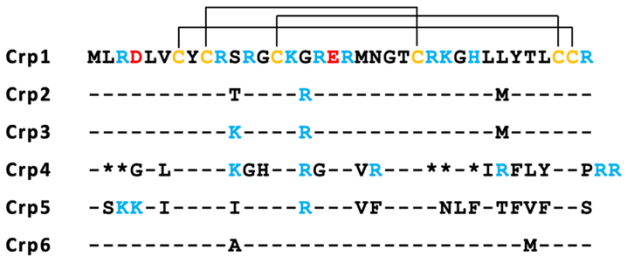

Fig. 1-1. Amino acid sequences of the six Crps. Some amino acid residues are color-coded as follows: Cys, yellow; Arg/Lys, blue; Glu/Asp, red. The three disulfide cross-links (cysteines 1–6, 2–4, 3–5) are also depicted. Dashes in lines of sequence indicate residues of identity with Crp1; and amino acids listed in lines of sequence indicate differences between each Crp and Crp1; asterisks in the Crp4 sequence indicate filler characters introduced to maximize the alignment.

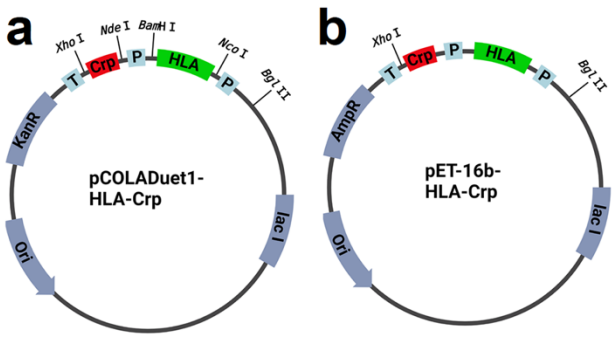

Fig. 1-2. Schematic representation of the expression vectors. (a) pCOLA-Duet1-HLA-Crp vector. (b) pET16b-HLA-Crp vector. P, T7 promoter; HLA, HLA gene; Crp, Crp gene; T, T7 terminator.

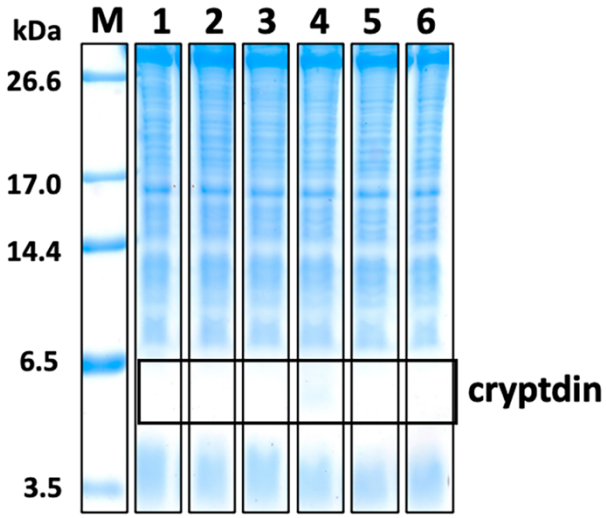

Fig. 1-3. Tricine-SDS-PAGE of Crp expression without partner protein using the BL21(DE3) strain. Lane M: marker; Lanes 1–6: whole-cell lysates of cryptdins 1–6.

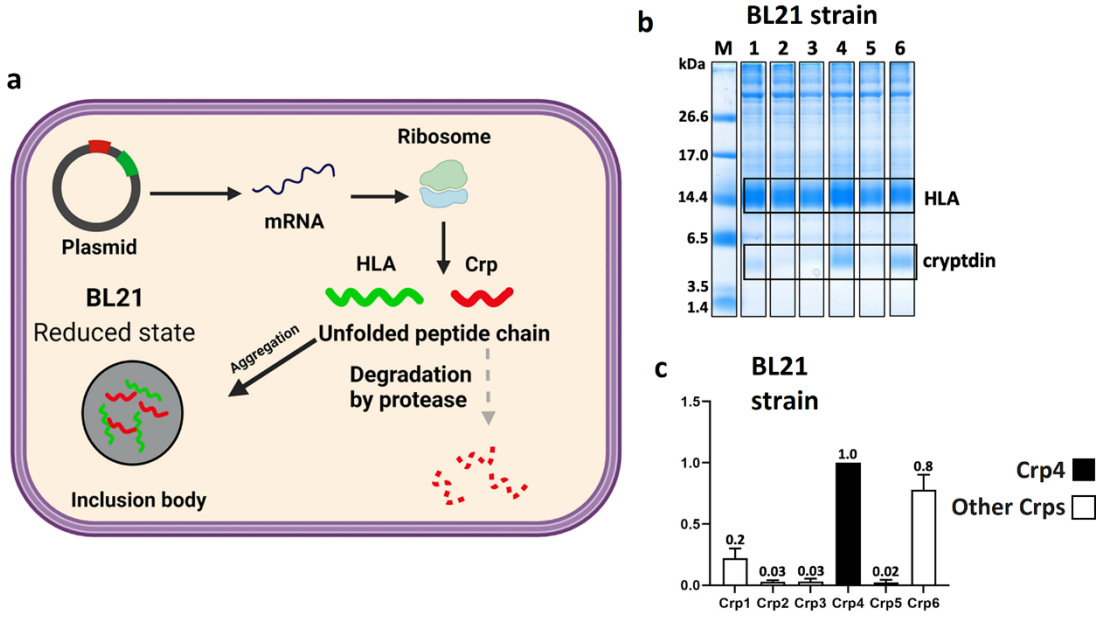

Fig. 1-4. Co-expression of Crps using the *E. coli* BL21(DE3) strain. (a) Schematic outline of the method for promoting inclusion body formation using the BL21(DE3) strain. HLA, green; Crp, red. When co-expressed with aggregation-prone HLA, Crp forms a stable inclusion body (black arrow). If it does not form, host proteases degraded the expressed Crp (gray arrows). (b) Tricine-SDS-PAGE results of the expression level of Crps. Lane M: marker; Lanes 1–6: precipitates of Crp1–6. (c) The intensity data of the expression of Crps relative to Crp4. n=3 for each.

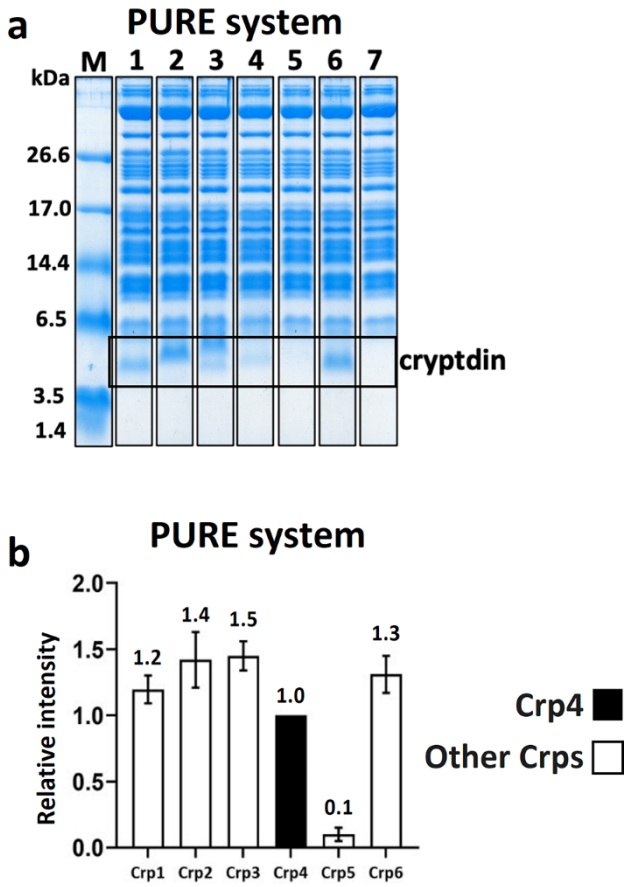

Fig. 1-5. Confirmation of the synthesis of Crps by ribosomes using the PURE system. (a) Tricine-SDS-PAGE results of the synthesis of Crps. Lane M: marker; Lanes 1–6: whole-cell lysates of Crp1–6; Lane 7: negative control. (b) The intensity data of the synthesis of Crps relative to Crp4. n=3 for each.

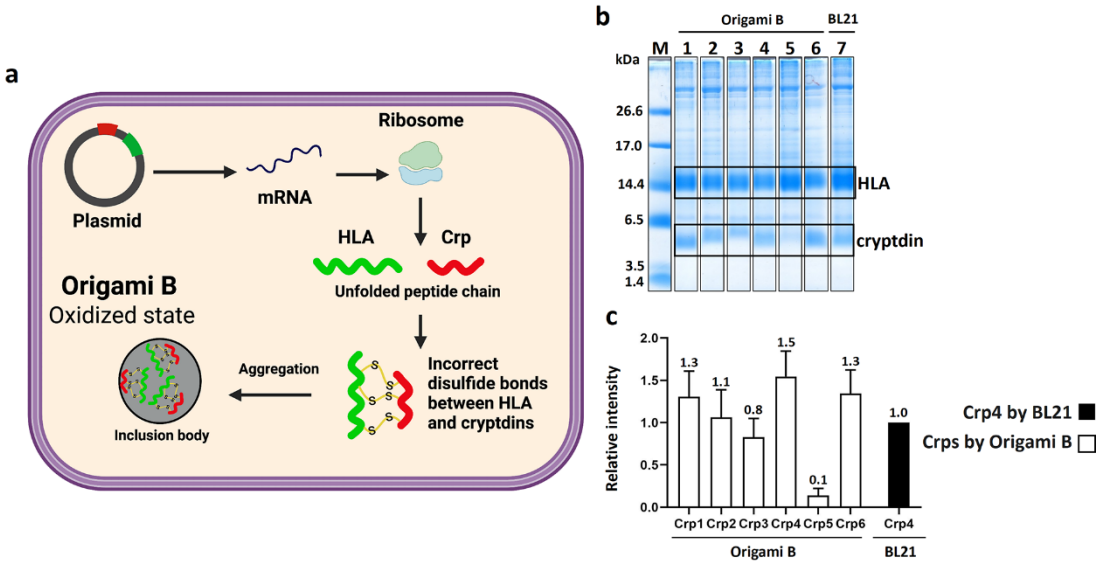

Fig. 1-6. Co-expression of Crps using the *E. coli* Origami™ B (DE3) strain. (a) Schematic outline of the newly investigated method for promoting inclusion body formation by disulfide bond cross-linking using the *E. coli* Origami™ B (DE3) strain. HLA, green; Crp, red; disulfide cross-link, yellow. Use of the Origami™ B (DE3) strain, which has an intracellular oxidative environment, as an expression host allows the formation of non-natural disulfide cross-links between aggregation-prone HLA and Crp. This is expected to result in more efficient inclusion body formation. (b) Tricine-SDS-PAGE results of the expression of Crps. Lane M: marker; Lanes 1–6: precipitates of Crp1–6. Lane7: Precipitate of Crp4 by BL21 strain was used as a control. (c) The intensity data of the expression of Crps relative to Crp4 using the BL21(DE3) strain. n=3 for each.

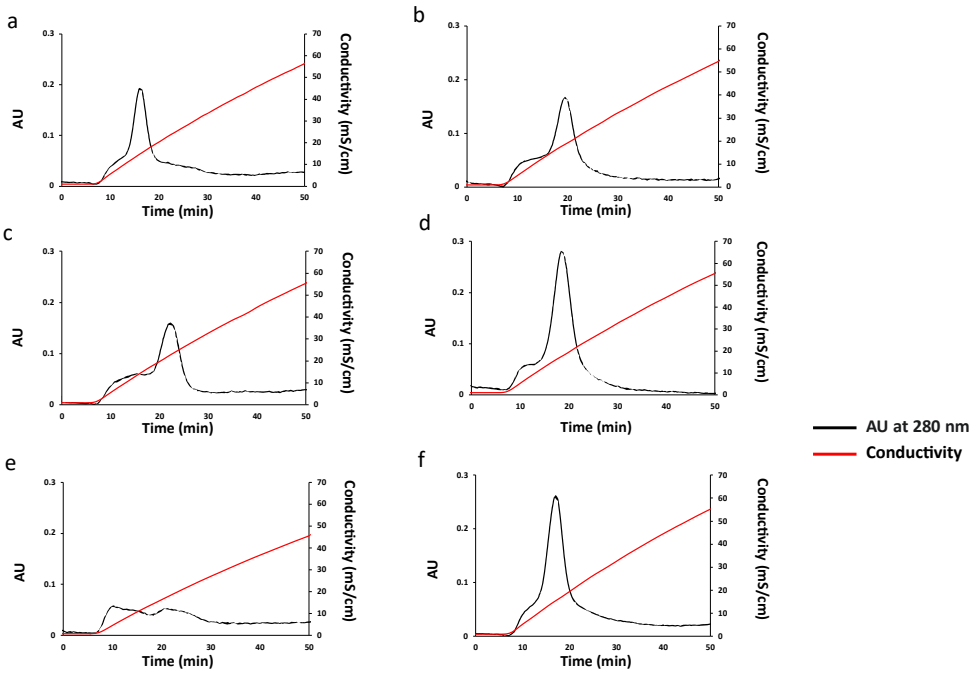

Fig. 1-7. Cation exchange chromatography (CIEX) results for Crps. (a) Crp1; (b) Crp2; (c) Crp3; (d) Crp4; (e) Crp5; and (f) Crp6.

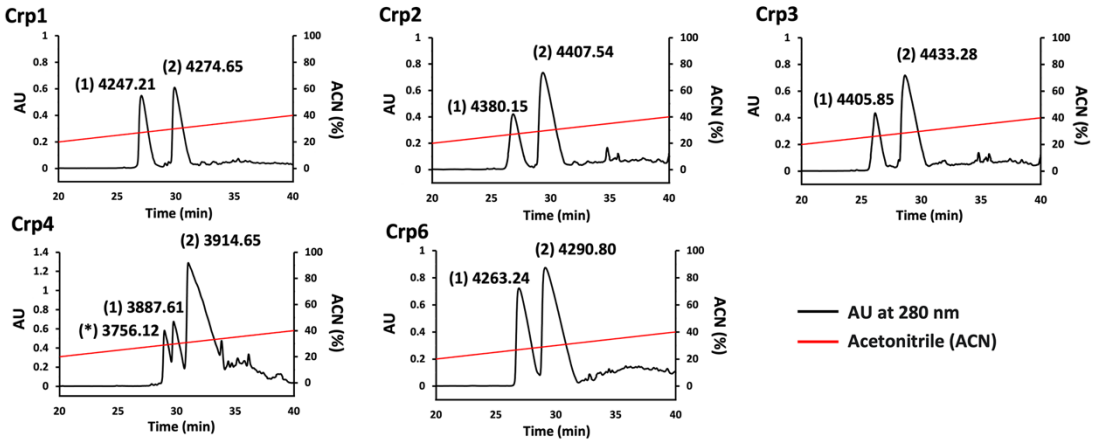

Fig. 1-8. Large-scale purification of refolded Crps by RP-HPLC. The molecular weight of each peak was determined by MALDI-TOF mass spectrometry. For Crp1, Crp2, Crp3, and Crp6, the two observable peaks are: (1) Crps; and (2) formyl Crps (due to the difference of approximately 28 Da determined by mass). For Crp4, the three observable peaks are: (*) Crp4 without methionine (due to the side chain length of the second amino acid of Crp4); (1) Crp4; and (2) formyl Crp4. Peptides produced in 500 mL of medium were loaded.

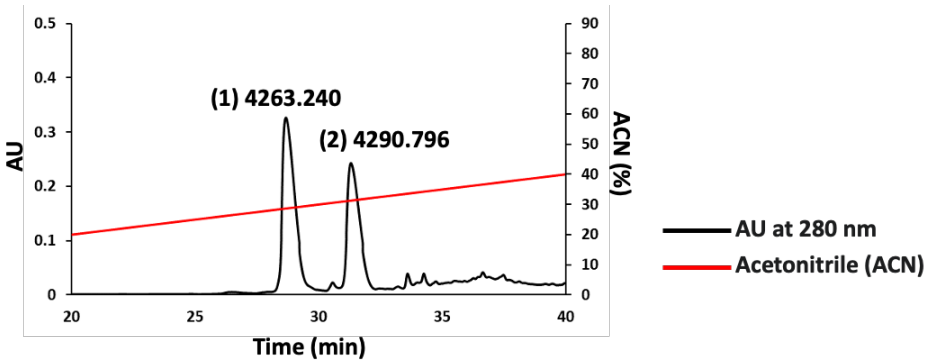

Fig. 1-9. RP-HPLC results after purification of Crp6 using the BL21 strain. The two observable peaks are: (1) Crp6; and (2) formyl Crp6. Compared with the result for Crp6 by using the Origami™ B strain (Fig. 1-8). the proportion of mature Crp6 was higher. Peptides produced in 1 L of medium were loaded.

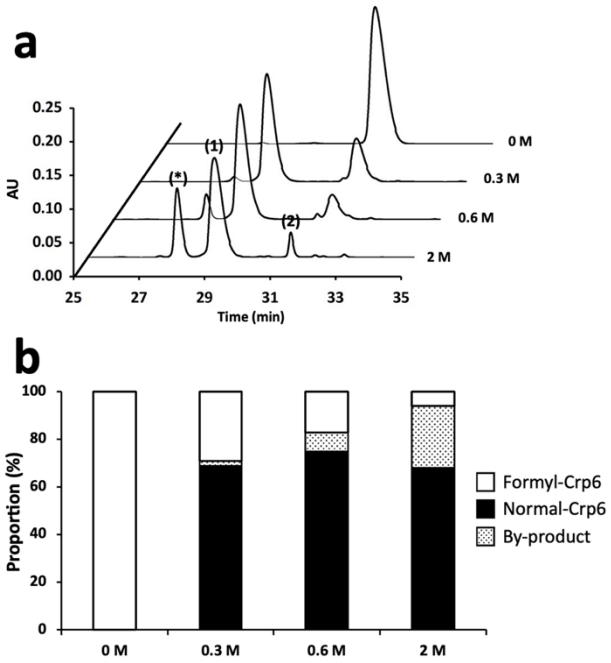

Fig. 1-10. The result of deformylation of Crp6 by acid hydrolysis. (a) RP- HPLC results of Crp6 treated with different concentrations of HCl, 0 (control), 0.3, 0.6, and 2 M HCl. The three observable peaks are: (*) by-product; (1); Crp6 after deformylation; and (2) undeformylated Crp6. (b) Bar graph showing the proportion of each product, confirmed by the peak area by RP-HPLC. The molecular weight of Crp6 was determined by MALDI- TOF mass spectrometry. Approximately 100 μg of Crp6 was loaded.

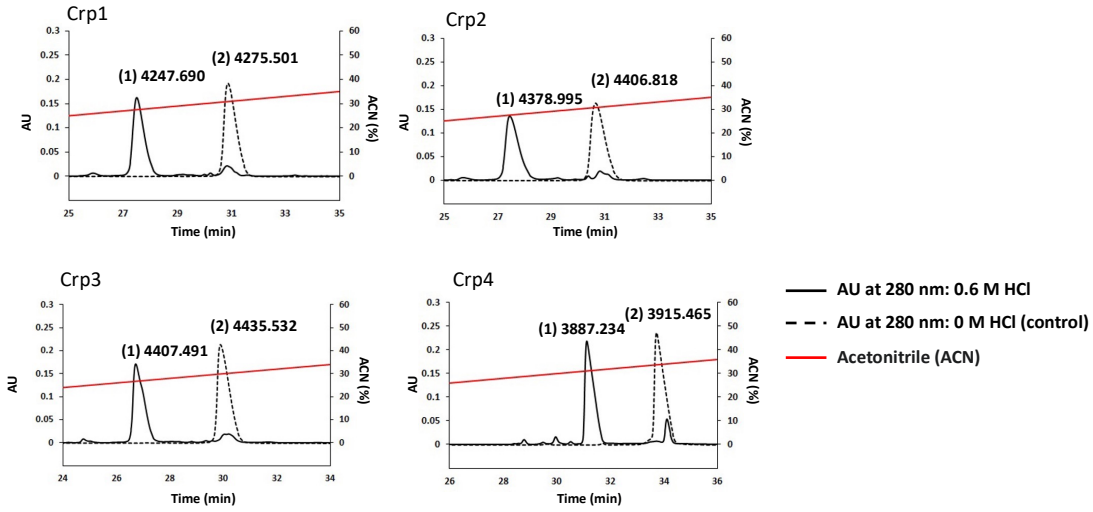

Fig. 1-11. RP-HPLC results for Crp deformylation. The figure shows the results for Crps treated with 0 M(control) and 0.6 M HCl. The two observable peaks are: (1) Crps after deformylation; and (2) undeformylated Crps. The molecular weight of the mature Crps was determined using MALDI-TOF mass spectrometry. Approximately 100 μg of Crps were loaded.

Chapter 2:

Structural information and antimicrobial activity of cryptdin family

2.1 Introduction

Defensins are small cysteine-rich cationic amphiphilic peptides that are widely distributed in plants (Belarmino LC et al., 2010), fungi (Zhu S, 2008), insects (Yi HY et al., 2014), and mammals (Meade KG et al., 2014; Kaiser V et al., 2000). Based primarily on the connectivity of six cysteine residues, mammalian defensins are divided into three subfamilies called alpha, beta, and theta-defensins. The human body contains six alpha-defensins, HNP1-4 (Ganz T et al., 1985; Selsted ME et al., 1985; Wilde CG et al., 1989), which are derived from human neutrophils, HD5 (Jones DE et al., 1992) and HD6 (Jones DE et al., 1993), which are derived from intestinal Paneth cells. At present, there are many studies on human α-defensins, revealing their structures (Szyk A et al., 2006; Wei G et al., 2010;), showing different antibacterial activities against different bacteria (Ericksen B et al., 2005), and the relationship between structure and antibacterial activity (Hu H et al., 2019; Rajabi M et al., 2012).

Cryptdin is an alpha defensin in mouse, which is different from human alpha defensins in that all six Crps are expressed in Paneth cells in the mouse small intestine (Ouellette AJ et al., 1996; Ouellette AJ et al., 1994). Paneth cells in mice respond immediately to multiple pathogenic stimuli, secrete cryptdin to kill pathogens, maintain the homeostasis of the mouse intestine, and provide positive effects on intestinal host defense (Ayabe T et al., 2000).

It has been reported that disulfide bonds play an important role in the antibacterial activity of cryptdin family (Maemoto A et al., 2004). Especially for Crp4, the oxidized and the reduced Crp4 showed a large difference in antibacterial activity against

commensal and noncommensal bacteria, and they also showed the difference in membrane disruption for these two types of bacteria (Masuda K et al., 2011). This might be related to the structural difference between the oxidized and the reduced Crp4 (Sato Y et al., 2022). Not only Crp4, but also the oxidized and the reduced Crp1 exhibited different antibacterial activities (Wang Q et al., 2022). The current research on the structure and function of the Crp family is limited to Crp4 (Rosengren KJ et al., 2006; Satchell DP et al., 2003; Jing W et al., 2004), but there is very little information related to the structure of other Crps. In addition, it has also been reported that Crp4 exhibited the strongest antibacterial activity *in vitro* (Ouellette AJ et al., 1994), but it is rare to compare the antibacterial activity of all Crps at the same time. Here, I used circular dichroism (CD) to reveal the structural changes of the oxidized and the reduced cryptdin family in different environments. In addition, I determined the antibacterial activity of the cryptdin family against different types of bacteria.

2.2 Materials and Methods

Preparation of the reduced cryptdin family

The various cryptdin families prepared in the Chapter 1 were reacted with 500mM Dithiothreitol (DTT) at 25 °C for 15 h. 10% TFA was used to adjust the solution to a pH between 2-3. The reacted Crps were purified by RP-HPLC using a COSMOSIL® Protein-R column (Nacalai Tesque). Elution was performed using a linear gradient of 0–50% acetonitrile and 0.1% TFA. Yields were calculated based on the absorbance at 280 nm. The molecular weights of the eluted Crps were determined by MALDI-TOF-MS (autoflex™ speed, Bruker).

Circular dichroism (CD) measurements

Circular dichroism (CD) data were collected using a Jasco J 725 spectropolarimeter (Jasco Inc.) for both the oxidized and the reduced cryptdin family. Spectra were collected from 250 to 190 nm and scanned at 20 nm/min at 25°C. The bandwidth was 1.0 nm, and each data point was scanned four times under nitrogen gas. The spectra were measured in three different environments: 10 mM phosphate-buffered saline (PBS), pH 7.4; 40% trifluoroethanol (TFE); and 10 mM sodium dodecyl sulfate (SDS).

The mean residue ellipticity values, θ, were calculated using the formula below:

$$\theta = \frac{\theta observed}{10 \times n \times C \times l} \quad (1)$$

where n is the number of amino acid residues, C is the peptide concentration, and l is the optical pass length of the cell.

Antimicrobial activity assay

Gram-positive bacteria (*Staphylococcus aureus*, ATCC6538p and *Listeria monocytogenes*, JCM 7671) and Gram-negative bacteria (*Escherichia coli,* ATCC43827 and *Salmonella enterica, JCM1652*) were used to test the antibacterial activity. Bacterial strains were cultured in 3% TSB medium (for *S. aureus, E. coli and S. enterica*) or BHI medium (for *L. monocytogenes*). After shaking at 37°C until the absorbance at 600 nm was 0.4, the cultures were centrifuged at 9300 × g for 5 min, and the pellets were washed twice with 10 mM PBS, (pH 7.4), resuspended, and diluted 10-fold (*E. coli*) and 20-fold with PBS (*S. aureus, S. enterica and L. monocytogenes*). The Crps prepared in the Chapter 1 were freeze-dried and diluted to the corresponding concentrations with PBS. The diluted bacteria (20 μL aliquots) were mixed with 20 μL of the diluted Crps, and the concentration of the bacteria was 1×10^7 CFU/mL. The mixtures were then incubated at 37°C for 1 h, diluted 1000 times, and 50 μL was added to solid medium containing 3% TSB or BHI. After overnight culturing at 37°C, the survival rate was calculated by colony counting (n=6 for each).

2.3 Results and Discussion

Comparison of steric structures by circular dichroism (CD)

To obtain information on the steric structures of the oxidized and reduced Crps (oxiCrps and redCrps), CD spectra were measured under different conditions, and the results are shown in Fig. 2-1 and Fig. 2-2. The steric structure of the oxiCrp4 has been studied previously using CD and NMR (Rosengren KJ et al., 2006; Satchell DP et al., 2003; Jing W et al., 2004), and it has been reported that the three disulfide bonds stabilize the three β-strands. Consistent with previous results, the oxiCrp4 in aqueous solution exhibited a negative maximum at approximately 200 nm and a broad positive maximum at approximately 225 nm (Fig. 2-1a). These spectral features were generally common in the other oxiCrps, suggesting that they form a conformation similar to that of the oxiCrp4. Furthermore, CD spectra were measured in highly hydrophobic (40% TFE) and membrane-mimetic (10 mM SDS) environments, but no significant changes in the spectra in aqueous solution were observed for any of the oxiCrps (Fig. 2-1b, c). This suggests that all of the oxiCrps had a stable secondary structure due to disulfide cross-linking and that their steric structures were stable in various environments. Under all measurement conditions, the CD spectrum of the oxiCrp4 exhibited a stronger broad peak at 225 nm compared to the other oxiCrps. Unfortunately, it is unclear at this time whether this reflects a difference in the steric structure associated with the antimicrobial spectrum characteristic of the oxiCrp4 or simply a difference in the primary sequence.

In contrast, the redCrps showed a different structure. The redCrps exhibits a random structure in an aqueous solution(Fig. 2-2a). Among them, although Crp6 was very

similar to Crp1-3 in primary structure (Fig. 2-3), its value at 200 nm was different from that of the other redCrps, but the reason was unclear. In addition, in the environment of 40% TFE and 10 mM SDS (Fig. 2-2b, c), the redCrps had a strong positive value at 190 nm and negative values at 208 nm and 222 nm, which were the same characteristics as the peptides with α-helix structure (Dong H et al., 2018; Liu H et al., 2015). Among them, the redCrp4 showed differences from the other four redCrps, indicating that the redCrp4 and the other redCrps may have different membrane interactions, and indicated that the redCrp4 may exhibit different activities from the other. But this still needs to be verified by more activity experiments of the reduced cryptdin family.

Comparison of the characteristics of the antimicrobial activity of Crps

The bactericidal activity of the oxidized Crps against Gram-positive bacteria (*S. aureus and L. monocytogenes*) and Gram-negative bacteria (*E. coli and S. enterica*) was analyzed. Crp4 exhibited the strongest antimicrobial activity against Gram-negative bacteria, followed by Crp3 and Crp2. Crp1 and Crp6 exhibited the weakest activities (Fig. 2-4). For instance, 5.0 μg/mL Crp3 or Crp4 was sufficient to kill all Gram-negative bacteria, but the same concentration of Crp1 or Crp6 could only kill 20% of *E. coli* and 50% of *S. enterica* . However, Crp4 exhibited very low activity against Gram-positive bacteria (Fig. 2-5). At a concentration of 10 μg/mL, it still only killed approximately 30% of *L. monocytogenes* and 10% of *S. aureus*. In contrast, the other four Crps all exhibited very strong bactericidal activity, with their minimum bactericidal concentration (MBC) values below 1.5 μg/mL against *S. aureus and 5*

μg/mL against *L. monocytogenes*, which was much lower than the MBC of these Crps against Gram-negative bacteria. These trends clearly indicate that each Crp isoform has a very different antimicrobial spectrum.

The number and variety of bacteria in different parts of the mouse small intestine vary. Paneth cells at the bottom of small intestinal crypts of the mouse respond immediately to stimulation by a variety of pathogens, including many different bacteria, to secrete intracellular granules rich in Crps (Ayabe T et al., 2000; Ayabe T et al., 2004; Nakamura K et al., 2016), killing pathogenic bacteria to contribute to innate immunity. It has been reported that different parts of the mouse small intestine also express each Crp isoform to different degrees (Nakamura K et al., 2020; Karlsson J et al., 2008; Darmoul D et al., 1996), suggesting that each Crp isoform may play a different role in the defense of the small intestine (Inoue R et al., 2008). For this reason, our finding that each Crp isoform exhibited a different antimicrobial spectrum is very interesting. To the best of our knowledge, no reports to date have directly or simultaneously compared the MBCs of many types of Crps. In the case of Gram-negative bacteria in this study, with the exception of Crp4, the other four Crps exhibited activities that were highly consistent with their electric charge (Table 2-1), indicating that in the case of Gram-negative bacteria, the activity exhibited by Crps is likely to be affected by the charge strength. The microbicidal activity of these four Crps (Crp1, Crp2, Crp3, and Crp6), but not Crp4, against *E. coli* was stronger the higher their positive charge (Table 1). These four Crp isoforms have a high degree of sequence homology, differing by only 2–3 amino acids (Fig. 2-3). This suggests that the activity of these Crps against Gram-

negative bacteria depends on the strength of their electrostatic interaction with the membrane and that the basic mechanism of action of membrane disruption is similar. Unlike Gram-negative bacteria, the activity of Crps against Gram-positive bacteria was not specifically related to their electric charge and differed largely between Crp4 and the other Crps. This particularly weak activity against Gram-positive bacteria may be because Crp4 has a sequence that is considerably different from the other Crps, and the mechanism of action is also different. Additionally, the antibacterial activity of Crp3 against bacteria was slightly stronger than that of Crp1, Crp2, and Crp6. The only primary sequence difference between Crp3 and Crp2 is at position 11 (Crp3 has a lysine and Crp2 has a threonine). It has been reported that amino acids at positions 11 and 16 of Crp1, Crp2, Crp3, and Crp6 are predicted to be located at conserved turns on the molecular surface based on analogy with HNP-1, HNP-3, NP-2, and NP-5 (Ouellette AJ et al., 1994; Lencer WI et al., 1997; Aley SB et al., 1994). Based on these findings, the amino acid at position 11 may affect the interaction between Crps (Crp1, Crp2, Crp3, and Crp6) and *S. aureus.*

2.4 References

Belarmino LC, Capriles PV, Crovella S, Dardene LE, Benko-Iseppon AM. EST-database search of plant defensins - an example using sugarcane, a large and complex genome. Curr Protein Pept Sci. 2010;11(3):248-54. https://doi.org/10.2174/138920310791112048

Zhu S. Discovery of six families of fungal defensin-like peptides provides insights into origin and evolution of the CSalphabeta defensins. Mol Immunol. 2008;45(3):828-38. https://doi.org/10.1016/j.molimm.2007.06.354

Yi HY, Chowdhury M, Huang YD, Yu XQ. Insect antimicrobial peptides and their applications. Appl Microbiol Biotechnol. 2014;98(13):5807-22. https://doi.org/10.1007/s00253-014-5792-6

Meade KG, Cormican P, Narciandi F, Lloyd A, O'Farrelly C. Bovine β-defensin gene family: opportunities to improve animal health? Physiol Genomics. 2014;46(1):17-28. https://doi.org/10.1152/physiolgenomics.00085.2013

Kaiser V, Diamond G. Expression of mammalian defensin genes. J Leukoc Biol. 2000;68(6):779-84.

Ganz T, Selsted ME, Szklarek D, Harwig SS, Daher K, Bainton DF, Lehrer RI. Defensins. Natural peptide antibiotics of human neutrophils. J Clin Invest. 1985 Oct;76(4):1427-35. https://doi.org/10.1172/JCI112120

Selsted ME, Harwig SS, Ganz T, Schilling JW, Lehrer RI. Primary structures of three human neutrophil defensins. J Clin Invest. 1985 Oct;76(4):1436-9. https://doi.org/10.1172/JCI112121

Wilde CG, Griffith JE, Marra MN, Snable JL, Scott RW. Purification and characterization of human neutrophil peptide 4, a novel member of the defensin family. J Biol Chem. 1989 Jul 5;264(19):11200-3

Jones DE, Bevins CL. Paneth cells of the human small intestine express an antimicrobial peptide gene. J Biol Chem. 1992 Nov 15;267(32):23216-25.

Jones DE, Bevins CL. Defensin-6 mRNA in human Paneth cells: implications for antimicrobial peptides in host defense of the human bowel. FEBS Lett. 1993 Jan 4;315(2):187-92. https://doi.org/10.1016/0014-5793(93)81160-2

Szyk A, Wu Z, Tucker K, Yang D, Lu W, Lubkowski J. Crystal structures of human alpha-defensins HNP4, HD5, and HD6. Protein Sci. 2006 Dec;15(12):2749-60. https://doi.org/10.1110/ps.062336606

Wei G, Pazgier M, de Leeuw E, Rajabi M, Li J, Zou G, Jung G, Yuan W, Lu WY, Lehrer RI, Lu W. Trp-26 imparts functional versatility to human alpha-defensin HNP1. J Biol Chem. 2010 May 21;285(21):16275-85. https://doi.org/10.1074/jbc.M110.102749

Ericksen B, Wu Z, Lu W, Lehrer RI. Antibacterial activity and specificity of the six human {alpha}-defensins. Antimicrob Agents Chemother. 2005 Jan;49(1):269-75. https://doi.org/10.1128/AAC.49.1.269-275.2005

Hu H, Di B, Tolbert WD, Gohain N, Yuan W, Gao P, Ma B, He Q, Pazgier M, Zhao L, Lu W. Systematic mutational analysis of human neutrophil α-defensin HNP4. Biochim Biophys Acta Biomembr. 2019 Apr 1;1861(4):835-844. https://doi.org/10.1016/j.bbamem.2019.01.007

Rajabi M, Ericksen B, Wu X, de Leeuw E, Zhao L, Pazgier M, Lu W. Functional determinants of human enteric α-defensin HD5: crucial role for hydrophobicity at dimer interface. J Biol Chem. 2012 Jun 22;287(26):21615-27. https://doi.org/10.1074/jbc.M112.367995

Ouellette AJ, Selsted ME. Paneth cell defensins: endogenous peptide components of intestinal host defense. FASEB J. 1996 Sep;10(11):1280-9. https://doi.org/10.1096/fasebj.10.11.8836041

Ouellette AJ, Hsieh MM, Nosek MT, Cano-Gauci DF, Huttner KM, Buick RN, Selsted ME. Mouse Paneth cell defensins: primary structures and antibacterial activities of numerous cryptdin isoforms. Infect Immun. 1994 Nov;62(11):5040-7. https://doi.org/10.1128/iai.62.11.5040-5047.1994

Ayabe T, Satchell DP, Wilson CL, Parks WC, Selsted ME, Ouellette AJ. Secretion of microbicidal α-defensins by intestinal Paneth cells in response to bacteria. Nat Immunol. 2000;1:113–8. https://doi.org/10.1038/77783

Maemoto A, Qu X, Rosengren KJ, Tanabe H, Henschen-Edman A, Craik DJ, Ouellette AJ. Functional analysis of the alpha-defensin disulfide array in mouse cryptdin-4. J Biol Chem. 2004 Oct 15;279(42):44188-96. https://doi.org/10.1074/jbc.M406154200

Masuda K, Sakai N, Nakamura K, Yoshioka S, Ayabe T. Bactericidal activity of mouse α-defensin cryptdin-4 predominantly affects noncommensal bacteria. J Innate Immun. 2011;3(3):315-26. https://doi.org/10.1159/000322037

Sato Y, Wang Y, Song Y, Geng W, Yan S, Nakamura K, Kikukawa T, Demura M, Ayabe T, Aizawa T. Potent bactericidal activity of reduced cryptdin-4 derived from its hydrophobicity and mediated by bacterial membrane disruption. Amino Acids. 2022 Feb;54(2):289-297. https://doi.org/10.1007/s00726-021-03115-3

Wang Q, Yang Y, Luo G, Zhou Y, Tolbert WD, Pazgier M, Liao C, Lu W. Mouse α-Defensins: Structural and Functional Analysis of the 17 Cryptdin Isoforms Identified from a Single Jejunal Crypt. Infect Immun. 2022 Dec 6:e0036122. https://doi.org/10.1007/s00726-021-03115-3

Rosengren KJ, Daly NL, Fornander LM, Jönsson LMH, Shirafuji Y, Qu X, et al. Structural and functional characterization of the conserved salt bridge in mammalian paneth cell α-defensins: Solution structures of mouse cryptdin-4 and (E15D)-cryptdin-4. J Biol Chem. 2006;281:28068–78. https://doi.org/10.1074/jbc.M604992200

Satchell DP, Sheynis T, Shirafuji Y, Kolusheva S, Ouellette AJ, Jelinek R. Interactions of mouse Paneth cell α-defensins and α-defensin precursors with membranes. Prosegment inhibition of peptide association with biomimetic membranes. J Biol Chem. Currently published by Elsevier Inc; originally published by American Society for Biochemistry and Molecular Biology. 2003;278:13838–46. http://doi.org/10.1074/jbc.M212115200

Jing W, Hunter HN, Tanabe H, Ouellette AJ, Vogel HJ. Solution structure of cryptdin-4, a mouse paneth cell α-defensin. Biochemistry. 2004;43:15759–66. https://doi.org/10.1021/bi048645p.

Dong N, Li XR, Xu XY, Lv YF, Li ZY, Shan AS, Wang JL. Characterization of bactericidal efficiency, cell selectivity, and mechanism of short interspecific hybrid peptides. Amino Acids. 2018 Apr;50(3-4):453-468. https://doi.org/10.1007/s00726-017-2531-1

Liu H, Lei M, Du X, Cui P, Zhang S. Identification of a novel antimicrobial peptide from amphioxus Branchiostoma japonicum by in silico and functional analyses. Sci Rep. 2015 Dec 18;5:18355. https://doi.org/10.1038/srep18355

Ayabe T, Ashida T, Kohgo Y, Kono T. The role of Paneth cells and their antimicrobial peptides in innate host defense. Trends Microbiol. 2004;12:394–8. https://doi.org/10.1016/j.tim.2004.06.007

Nakamura K, Sakuragi N, Takakuwa A, Ayabe T. Paneth cell α-defensins and enteric microbiota in health and disease. Biosci Microbiota Food Health. 2016;35:57–67. https://doi.org/10.12938/bmfh.2015-019

Karlsson J, Pütsep K, Chu H, Kays RJ, Bevins CL, Andersson M. Regional variations in Paneth cell antimicrobial peptide expression along the mouse intestinal tract. BMC Immunol. 2008;9:37. https://doi.org/10.1186/1471-2172-9-37

Darmoul D, Ouellette AJ. Positional specificity of defensin gene expression reveals Paneth cell heterogeneity in mouse small intestine. Am J Physiol. 1996;271:G68–74. https://doi.org/10.1152/ajpgi.1996.271.1.G68

Aley SB, Zimmerman M, Hetsko M, Selsted ME, Gillin FD. Killing of Giardia lamblia by cryptdins and cationic neutrophil peptides. Infect Immun. 1994;62:5397–403. https://doi.org/10.1128/iai.62.12.5397-5403.1994

Lencer WI, Cheung G, Strohmeier GR, Currie MG, Ouellette AJ, Selsted ME, et al. Induction of epithelial chloride secretion by channel-forming cryptdins 2 and 3. Proc Natl Acad Sci U S A. 1997;94:8585–9. https://doi.org/10.1073/pnas.94.16.8585

Table 2-1 Characteristics of cryptdins.

Crps	Mw	PI	GRAVY score	Charge*
Crp1	4253.12	9.61	-0.483	+7
Crp2	4384.32	9.86	-0.647	+8
Crp3	4411.39	9.99	-0.736	+9
Crp4	3886.55	9.86	-0.397	+8
Crp5	4339.32	9.86	0.169	+8
Crp6	4267.21	9.61	-0.339	+7

Molecular weight of fully reduced form (Mw), isoelectric point (pI), and grand average of hydropathy (GRAVY). *The charge was calculated from the following values at pH 7.4: Asp, -1; Glu, -1; Arg, +1; Lys, +1.

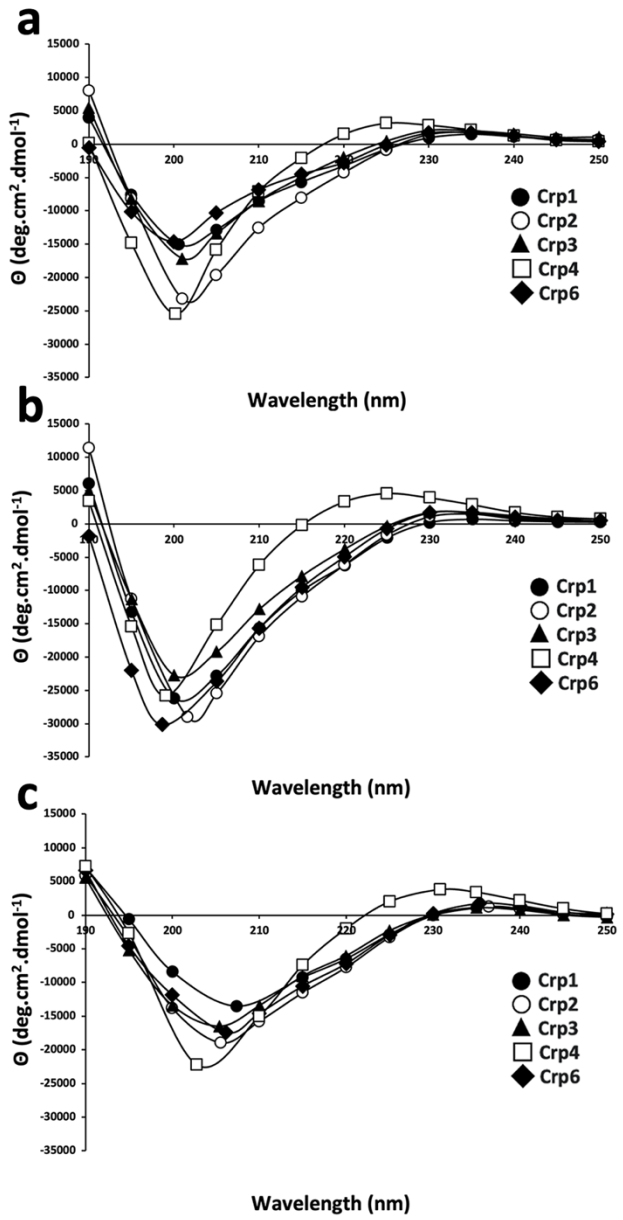

Fig. 2-1. Circular dichroism (CD) spectra for oxidized Crps measured from 280 to 190 nm at 25℃. Each peptide, at 30 μM, was measured in (a) 10 mM phosphate-buffered saline (PBS, pH 7.4); (b) 40% trifluoroethanol (TFE); (c) 10 mM sodium dodecyl sulfate (SDS).

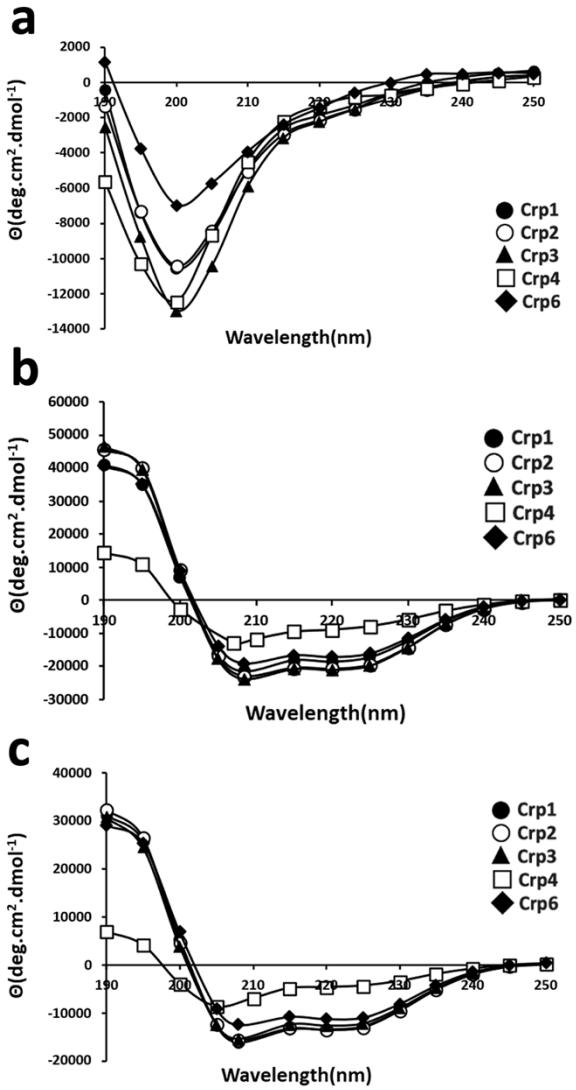

Fig. 2-2. Circular dichroism (CD) spectra for reduced Crps measured from 280 to 190 nm at 25℃. Each peptide, at 30 μM, was measured in (a) 10 mM phosphate-buffered saline (PBS, pH 7.4); (b) 40% trifluoroethanol (TFE); (c) 10 mM sodium dodecyl sulfate (SDS).

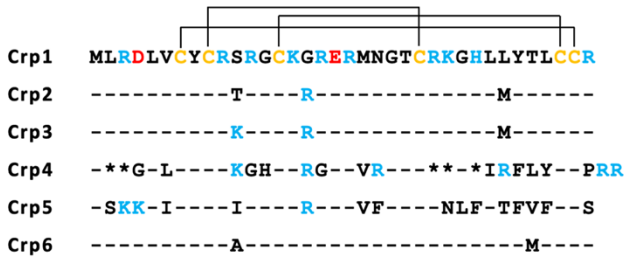

Fig. 2-3. Amino acid sequences of the six Crps. Some amino acid residues are color-coded as follows: Cys, yellow; Arg/Lys, blue; Glu/Asp, red. The three disulfide cross-links (cysteines 1–6, 2–4, 3–5) are also depicted. Dashes in lines of sequence indicate residues of identity with Crp1; and amino acids listed in lines of sequence indicate differences between each Crp and Crp1; asterisks in the Crp4 sequence indicate filler characters introduced to maximize the alignment.

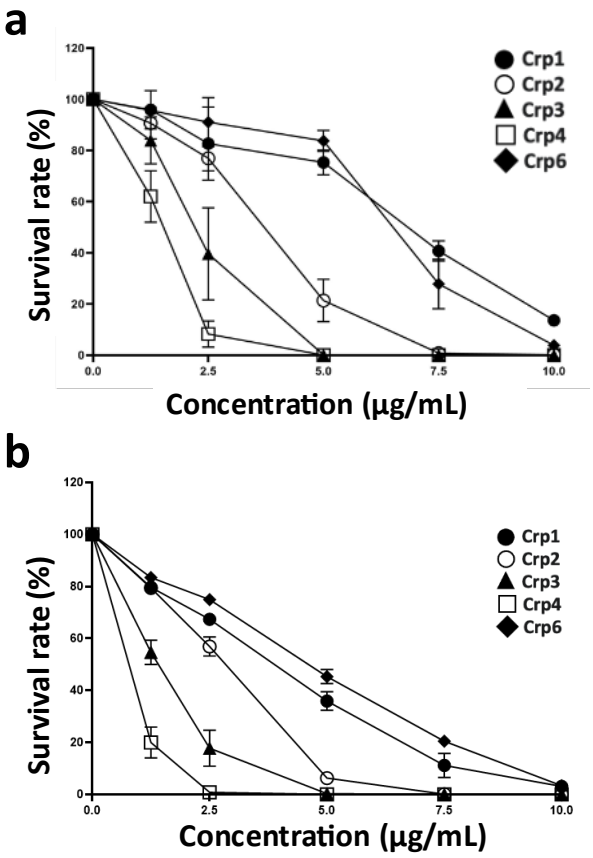

Fig. 2-4. Antimicrobial activity of Crps against Gram-negative bacteria. (a) Approximately 1×10^7 CFU/mL *E. coli* was exposed to peptides at 0, 1.25, 2.5, 5, 7.5, and 10 μg/mL; (b) Approximately 1×10^7 CFU/mL *S. enterica* was exposed to peptides at 0, 1.25, 2.5, 5, 7.5, and 10 μg/mL. Data are presented as means ± the standard error of the mean (SEM). n=6 for both (a) and (b).

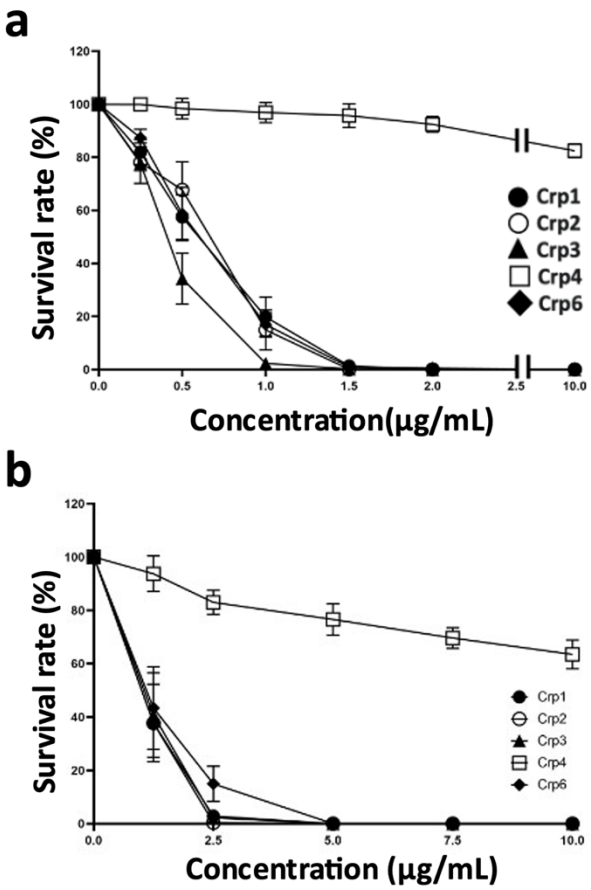

Fig. 2-5. Antimicrobial activity of Crps against Gram-positive bacteria. (a) Approximately 1×10^7 CFU/mL *S. aureus* was exposed to peptides at 0, 0.25, 0.5, 1, 1.5, 2 and 10 μg/mL; (b) Approximately 1×10^7 CFU/mL *L. monocytogenes* was exposed to peptides at 0, 1.25, 2.5, 5.0, 7.5and 10 μg/mL. Data are presented as means ± the standard error of the mean (SEM). n=6 for both (a) and (b).

Conclusion

In this study, to form inclusion bodies so as to avoid degradation of cysteine-containing antimicrobial peptides, we devised a method involving the use of *E. coli* with an oxidative intracellular environment and applied it to the production of the Crp family of peptides. This approach allowed successful production of five recombinant Crp isoforms. Crp5, which could not be produced, was found to be limited by a low level of synthesis at the ribosomal level. Although *E. coli* strains with an oxidative intracellular environment produced peptides with a formyl group on the N-terminal methionine, I showed that deformylation by hydrolysis under acidic conditions was effective at increasing production. The Crp family of peptides obtained using this experimental system exhibited significant differences in their antimicrobial spectra, even though their basic steric structures appeared to be similar. The expression system developed in this study is expected to elucidate the mechanism of action responsible for differences in the antimicrobial spectrum of the Crp family of peptides. In particular, the production of peptides labeled with ^{15}N and ^{13}C stable isotopes using this expression system is expected to be useful for future detailed structure and interaction analyses by NMR.

Acknowledgments

I gratefully acknowledge the invaluable suggestions and support of Professor Tomoyasu Aizawa. I would also like to express my gratitude to Professor Tokiyoshi Ayabe, Associate Professor Takashi Kikukawa, Assistant Professor Takashi Tsukamoto for their helpful suggestions and support. I also deeply thank my fellow students for their many advice, discussion, support and kindness in my experiments as well as in my daily life. Finally, I would like to express grateful appreciation to my family for many support and encouragement during my campus life in Hokkaido University.